JOURNAL OF AGRICULTURAL AND FOOD CHEMISTRY
ARTICLE

J. Agric. Food Chem. **2009,** *57,* 6803–6814 **6803**
DOI:10.1021/jf900832g

Mechanism and Related Kinetics of 5-Methyltetrahydrofolic Acid Degradation during Combined High Hydrostatic Pressure−Thermal Treatments

Philippe H. C. J. Verlinde,[†] Indrawati Oey,[†] Wim M. Deborggraeve,[‡] Marc E. Hendrickx,[†] and Ann M. Van Loey*,[†]

[†]Laboratory of Food Technology and Leuven Food Science and Nutrition Research Centre (LFoRCe), Department of Microbial and Molecular Systems (M2S), Katholieke Universiteit Leuven, Kasteelpark Arenberg 22, Box 2457, 3001 Leuven, Belgium, and [‡]Division of Molecular Design and Synthesis, Department of Chemistry, Katholieke Universiteit Leuven, Celestijnenlaan 200F, Box 2404, B-3001 Leuven, Belgium

The mechanism and kinetics of the degradation of 5-methyltetrahydrofolic acid during thermal and combined high pressure−thermal treatments in an aqueous solution were investigated. In a first approach the degradation was described by a first-order kinetic model using single-response modeling, and the combined pressure−temperature dependence of the resulting degradation rate constants was empirically described. To obtain a mechanistic insight, degradation products were purified and identified by LC-MS and NMR. Quantification of an *s*-triazine derivative, 5-methyldihydrofolic acid, and *p*-aminobenzoyl-L-glutamate as predominant degradation products at atmospheric pressure resulted in elucidation and kinetic characterization of the folate degradation mechanism by Bayesian multiresponse modeling. The postulated mechanism was evaluated at elevated hydrostatic pressure. On the basis of the pressure and temperature dependence of the reaction rates, some degradation reactions were either accelerated or decelerated upon application of pressure. Multiresponse kinetics can be a valuable tool to assess the impact of high hydrostatic pressure and other processing techniques on nutrients, and incorporating mechanistic insights can advance the current kinetic approach for process optimization.

KEYWORDS: Nutrient degradation; folate; multiresponse modeling; high pressure; temperature; kinetics

INTRODUCTION

Since the late 1980s, high hydrostatic pressure processing has attracted considerable interest in food research because the technology enables some novel and diverse uses combined with key advantages over traditional (i.e., thermal) processing techniques. High hydrostatic pressure technology can induce destruction of microorganisms at moderate temperatures (*1*) and has been applied as a promising pasteurization technique for a broad range of food products. Application of hydrostatic pressure at moderate temperatures (HP/T treatments) may affect non-covalent bonds, whereas covalent bonds are mostly considered to be unaffected because phenomena accompanied by a decrease in volume are enhanced by pressure and vice versa according to the principle of le Chatelier (*2*−*4*). Several studies on micronutrient stability have shown that HP/T treatments insignificantly, or only slightly, affect the content of some vitamins in fruit- and vegetable-based products (*5*−*8*). This trend cannot be generalized for all micronutrients because HP/T treatments cause significant losses of water-soluble vitamins such as folates (*9*−*13*).

*Corresponding author (telephone +32 16 321567; fax +32 16 321960; e-mail ann.vanloey@biw.kuleuven.be).

Folates are attracting considerable interest in the field of nutrition due to the growing amount of evidence pointing to the contribution of inadequate folate intake to severe health disorders such as neural tube defects (*14*), cardiovascular disease (*15*), neuropsychiatric conditions (*16*), and some types of cancer (*17*). In contrast to folic acid, the fully oxidized synthetic form of the vitamin, natural folates occur as 5,6,7,8-Tetrahydropteridines that are more prone to oxidative degradation. Cleavage of the C(9)−N(10) covalent bond in folic acid results in irreversible loss of vitamin activity (*18*, *19*) and has been postulated to occur during thermal and HP/T treatments (up to 600 MPa and 60 °C) (*9*−*12*). In general, folate degradation was mostly characterized by a negative activation volume as degradation rate constants were enhanced by increasing pressure at given temperatures (*9*−*12*). Because antioxidants such as ascorbate retard the pressure degradation of folates, it has been suggested that HP/T degradation of folates might be caused by oxidation (*11*, *20*), but in-depth knowledge of the chemical mechanism governing folate degradation under pressure is lacking.

In the current study, the stability of the predominantly occurring natural folate derivate, that is, [6*S*]5-methyltetrahydrofolic acid (**1**; **Figure 1**), was investigated under pressure in aqueous

Published on Web 07/02/2009

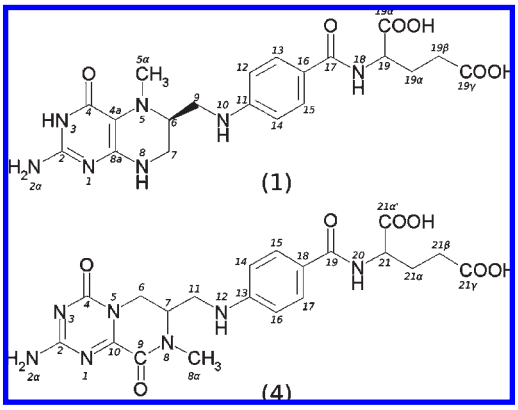

Figure 1. Atom numbering for **1** (top) and **4** (bottom).

solution. At first, degradation of **1** during HP/T treatments was characterized by single-response modeling to identify the pressure−temperature−time range of interest. Second, predominant degradation products were purified and identified to postulate possible degradation mechanisms and to enable quantification of these components. This knowledge was subsequently used to elucidate the degradation mechanism at atmospheric pressure using multiresponse kinetic modeling with Bayesian estimation. Because pressure and temperature changes cannot be the cause of entirely new reaction mechanisms (*21*), the obtained mechanism served as a starting point for validation and kinetic characterization of the mechanism under pressure. Application of multiresponse kinetics may overcome the incoherence of kinetic parameters reported in previous investigations (*9*−*12*) and serve as a basis to design an appropriate kinetic model to describe the pressure−temperature dependence of folate degradation (*12*).

The main purpose of this research was to perform a detailed study on folate degradation during thermal and HP/T treatments using a multiresponse modeling approach. This approach allowed us to gain insight and quantitatively describe the mechanism behind the previously reported pressure effect on folate stability (*9*−*12*). The application of multiresponse modeling to elucidate reaction mechanisms and kinetics is novel in the field of HP/T processing and contributes to the understanding of vitamin degradation occurring during HP/T processing.

MATERIALS AND METHODS

Materials. All chemicals and reagents used were of analytical or HPLC grade purity. [6*S*]5-Methyltetrahydrofolic acid (**1**) was donated as Ca and Na salt by Eprova AG (Schaffhausen, Switzerland). 5-Methyldihydrofolic acid (**2**; **Figure 2**) and *p*-aminobenzoyl-L-glutamic acid (**3**; **Figure 2**) were purchased from Schircks Laboratories (Jona, Switzerland) and stored in ampules under argon atmosphere at −80 °C. All solutions were prepared using reagent grade water (18 MΩ, 25 °C, Simplicity Water Purification System, Millipore, Molsheim, France).

Sample Preparation. For each experiment, samples of **1** (0.2−20 μg/mL, ≈0.4−40 μM) were freshly dissolved in water. To prevent variability in initial oxygen content, all solutions were thermostated at 25 °C and flushed with humidified air (0.35 L min^{-1}, 20 min, 25 °C). With precaution taken to avoid the inclusion of air bubbles, samples with a standardized oxygen content of 228−258 μM were filled in glass crimp-cap vials with rubber septa (800 μL, 8.2 × 30 mm, Cleanpack, Belgium) or flexible polyethylene tubes (400 μL, Bioplastic, Landgraaf, The Netherlands) for thermal and HP/T treatments, respectively. Contamination with pressure-transmitting medium during HP/T experiments was prevented by covering samples with a barrier film (Parafilm M) and double-vacuum-packaging the filled tubes at 1.1 Pa in polyethylene bags using a vacuum sealing machine (Multivac A300/16, Wolfertschwenden, Germany). Samples were stored on ice (0−4 °C) for a maximum of 15 min before treatments or analysis. To avoid UV-induced photodegradation, samples were wrapped in aluminum foil and preparative and treatment procedures were carried out under subdued light. Initial concentrations of **1** and **2** in samples were spectrophotometrically determined (*22*). Only samples with a UV absorbance ratio (A_{290nm}/A_{245nm}) of > 3.3 were used in this investigation.

Treatments. For thermal treatments (0.1 MPa) at 25−90 °C, samples were immersed in a water bath during preset time intervals of 0−420 min. Experiments at 90−100 °C were performed using silicone oil (M1028/50, Roger Coulon, Brussels, Belgium) as heating medium. For each heat treatment, a representative sample temperature−time profile was measured in duplicate during the heating, treatment, and subsequent cooling phase. Temperature was registered at the center of the closed vials at defined time intervals (2 s) using thermocouples (type T, Thermo Electric Benelux, Balen, Belgium) connected to a data logger (TM 9616, Ellab, Roedovre, Denmark).

For HP/T treatments at 35−65 °C and 100−800 MPa, experiments were conducted using a laboratory pilot scale, multivessel, high-pressure apparatus (Resato, Roden, The Netherlands) consisting of six (43 mL) or eight (8 mL) thermostated pressure reactors, with a propylene glycol mixture (Resato PG fluid, Resato) as pressure-transmitting medium. Before pressurization, the time required to insert the samples and close the reactors was standardized at 45 s. Pressure was built up at a constant rate of 100 MPa min^{-1}, and an equilibration period of 5 min was taken into account to allow the temperature inside the reactors to evolve back to the desired value after adiabatic heating. The latter time point was considered as the starting time for isothermal−isobaric conditions in kinetic experiments (time t_0). Pressure reactors were subsequently decompressed at defined time intervals between 5 and 60 min and samples removed 45 s after decompression. After thermal and HP/T treatments, samples were immediately immersed in ice water (0−4 °C) to eliminate further degradation reactions prior to HPLC analysis.

Chromatographic Methods. For preliminary single-response modeling experiments, concentrations of **1** (0−0.4 μM) were determined by gradient elution reversed-phase HPLC as described earlier (*11*). The apparatus consisted of an ÄKTA purifier chromatograph (GE Healthcare, Üppsala, Sweden) equipped with fluorescence detection (RF-10AxL, Shimadzu, Kyoto, Japan). Chromatography was performed at 25 °C using an analytical Prevail RP C_{18} column (250 × 4.6 mm, 5 μm particle size; Grace, Deerfield, IL), protected with guard cartridge (7.5 × 4.6 mm, 5 μm particle size). Fluorescence detection was applied at excitation and emission wavelengths of,respectively, 295 and 359 nm, with a sensitivity magnification factor of 128. For gradient elution, solvents were 5% (v/v) acetonitrile in 330 mM orthophosphoric acid (pH 2.1, solvent A) and 60% (v/v) acetonitrile in 330 mM orthophosphoric acid (pH 2.1, solvent B) at a flow rate of 1 mL min^{-1}. Prior to injection (100 μL), the column was equilibrated with 1 column volume (CV) of solvent A. Following injection, solvent A was maintained for 1 CV, and subsequently the concentration of B was linearly increased to 100% in 2 CVs. Mobile phase B was then maintained for 1 CV, and the column was re-equilibrated with 2 CVs of 100% mobile phase A. Quantification of **1** was performed using external calibration curves based on peak area and height.

Quantitative analysis of **1** (0−40 μM) and its degradation products for multiresponse modeling was performed using a 1200 series chromatograph (Agilent Technologies, Diegem, Belgium) equipped with a 1200 series UV-DAD detector. Components were separated at 25 °C on the aforementioned column using 0.1% formic acid (solvent C) and methanol (solvent D). Prior to injection (100 μL for samples, 1−100 μL for calibration curves), the column was equilibrated with 1 CV of 12% methanol (v/v, C/D) at a flow rate of 1 mL min^{-1}. After injection, components were eluted for 1 CV using 12% methanol, followed by a linear gradient to 56% methanol (v/v, C/D) in 3 CVs. Subsequently, the column was washed with 56% methanol for 2 CVs. Quantification of components was performed using external calibration curves based on peak area and height.

For LC-MS analysis of unknown degradation products the previous method was applied at an injection volume of 2−20 μL and a flow rate of 0.5 mL min^{-1} on a Zorbax XDBC18 column (150 × 4.6 mm, 5 μm particle size; Agilent Technologies) using a 1100 series chromatograph (Agilent Technologies) equipped with an LCQ Advantage Ion Trap mass spectrometer (Thermo Electron Co., Boston, MA). The spectrometer was operated in full-scan mode (*m*/*e* 100−1300) using positive electrospray ionization (ESI) with spray and capillary voltage of +5.5 kV and 24.4 V, respectively. The capillary temperature was 200 °C using nitrogen as sheath gas (80 mL min^{-1}). For MS-MS, the capillary temperature was

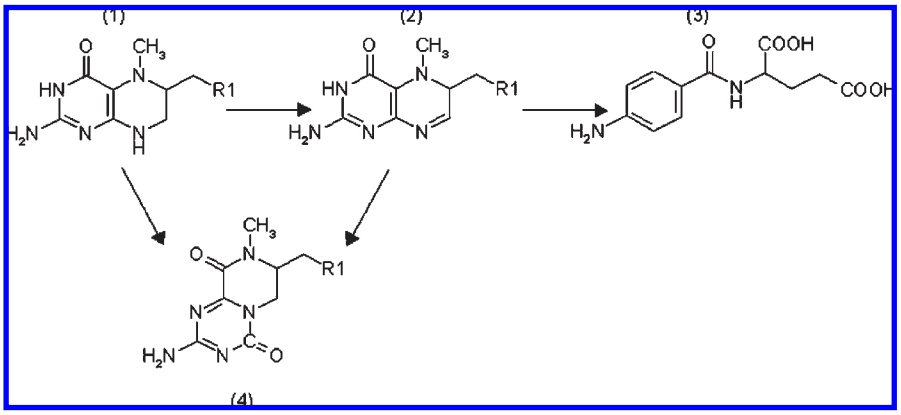

Figure 2. Revised 5-methyltetrahydrofolic acid oxidation mechanism of Blair et al. (*27*) according to the current spectral data. R_1 represents the *p*-aminobenzoyl-L-glutamate part of the molecules.

raised to 375 °C, and components (precursor ion ± 1 *m*/*e*) were subjected to a collision-induced dissociation (CID) source energy of 25%.

Purification of 5-Methyltetrahydrofolic Acid and Its Predominant Degradation Product. For the synthesis of degradation products, **1** (≈4 mM) was incubated in a closed vessel for 24 h at 100 °C and regularly shaken. Purification was achieved by scaling up the LC-MS method to a semipreparative method using a Prevail RP C_{18} column (250 × 10 mm, 5 μm particle size; Grace) on an ÄKTA purifier chromatograph (GE Healthcare). The injection volume was 500 μL and the flow rate, 5.0 mL min^{-1}. Fractionation was performed on the basis of the absorbance at 290 nm. Peaks with retention times at, respectively, 14.25, 17.66, 18.62, 19.58, and 22.34 min were pooled from 16 runs. Upon collection, fractions were frozen using liquid nitrogen and stored at −80 °C. Finally, solutions were lyophilized for 24 h, and the purified components were stored in capped vials under nitrogen atmosphere in a desiccator containing P_2O_5. The purity of lyophilized fractions was determined by LC-MS. To avoid photodegradation, all samples were wrapped in aluminum foil during storage. Spectral identification of components was performed in 15 μL of $^2H_6$-DMSO using a Bruker Avance 600 MHz spectrometer (Bruker Belgium, Brussels, Belgium) with a 1 mm MicroProbe (Bruker).

The reference component **1** (**Figure 1**) was obtained as free acid, appearing as a light brown solid: ^{1}H NMR ($^2H_6$-DMSO COSY) δ 1.86−1.96 [1 H, m, H−C(19β)], 2.01−2.09 [1 H, m, H−C(19β)], 2.31 [2 H, t, H_2−C(19α), *J* = 7.3 Hz], 2.49 [3 H, s, H_3−C(5α)], 2.77−2.81 [1 H, m, H_2−C(9)], 2.84−2.90 [1 H, m, H_2−C(9)], 2.91−2.95 [1 H, m, H−C(6)], 3.17 [m, H_2−C(7)], 4.34 [1 H, q, H−C(19), *J* = 7.3 Hz], 5.87 [2 H, s, H_2−N(2α)], 6.44 [1 H, m, H−N(8)], 6.56 [2 H, d, H−C(12) H−C(14), *J* = 8.6 Hz], 7.65 [2 H, d, H−C(13) H−C(15), *J* = 8.5 Hz], 8.06 [1 H, d, H−N(18), *J* = 7.4 Hz], 9.91 [1 H, s, H−N(3)]; ^{13}C NMR ($^2H_6$-DMSO, APT, HSQC, HMBC) δ 26.74 [C(19α)], 31.17 [C(19β)], 35.90 [C(7)], 43.11 [C(5α)], 43.99 [C(9)], 52.27 [C(19)], 55.71 [C(6)], 100.39 [C(4a)], 111.23 [C(12), C(14)], 120.99 [C(16)], 129.49 [C(13), C(15)], 151.55 [C(11)], 151.81 [C(8a)], 153.33 [C(2)], 159.14 [C(4)], 166.74 [C(17)], 174.49 [C(19α′)], 177.40 [C(18γ)]; ESI-MS [M + H] (positive ion mode) *m*/*e* 460; UV λ_{max} 289 ± 2 nm with ε = 23.8 × 10^3 cm^{-1} mol^{-1} L in phosphate buffer (0.1 M, pH 7.0); purity = 98.6% (relative area at 290 nm upon HPLC analysis).

The main degradation product was characterized as 2-amino-8-methyl-4,9-dioxo-7-methyl-*p*-aminobenzoylglutamate-6,7,8,9-tetrahydro-4*H*-pyrazino(1,2-*a*)-*s*-triazine (**4**; **Figure 1**) and was obtained as a bright yellow solid: ^{1}H NMR ($^2H_6$-DMSO COSY) δ 1.89−1.95 [1 H, m, H_2−C(21α), *J* = 7.4 Hz], 2.00−2.05 [1 H, m, H_2−C(21α)], 2.30 [2 H, t, H_2−C(21β), *J* = 7.4 Hz], 3.06 [3 H, s, H_3−C(8α)], 3.30−3.39 [2 H, m, H_2−C(11)], 3.77 [1 H, dd, H_S−C(6), *J* = 14.2 Hz, *J* = 4.7 Hz], 3.91 [1 H, m, H−C(7)], 4.31 [1 H, q, H−C(21), *J* = 7.0 Hz], 4.38 [1 H, d, H_R−C(6), *J*=14.0 Hz], 6.39 [1 H, t, H−N(12), *J* = 6.3 Hz], 6.56 [2 H, d, H−C(14) H−C(16), *J* = 8.5 Hz], 7.62 [2 H, d, H−C(15) H−C(17), *J* = 8.5 Hz], 8.06 [1 H, d, H−N(20), *J* = 7.3 Hz]; ^{13}C NMR ($^2H_6$-DMSO, APT, HSQC, HMBC) δ 26.77 [C(21α)], 31.14 [C(21β)], 35.03 [C(8α)], 41.01 [C(6)], 43.11 [C(11)], 52.50 [C(21)], 54.44 [C(7)], 111.23 [C(14), C(16)], 129.35 [C(15), C(17)], 151.10 [C(13)], 154.20 [C(2)], 154.44 [C(4)], 155.71 [C(9)], 156.87 [C(10)], 166.37 [C(19)], 173.80 [C(21α′)], 177.40 [C(21γ)] ; ESI-MS [M + H] (positive ion mode) *m*/*e* 474; UV λ_{max} 279 ± 1 nm with ε = 22.7 × 10^3 cm^{-1} mol^{-1} L in phosphate buffer (0.1 M, pH 7.0); purity = 96.3% (relative area at 290 nm upon HPLC analysis).

Data Analysis. Single-Response Kinetic Modeling. Previous studies have shown that in excess of oxygen, degradation kinetics of **1** can be described by apparent first-order reaction kinetics under isothermal/isobaric conditions (*9*, *11*, *12*). Hereto, the degradation was preliminarily described in a single-response modeling approach using eq 1, with *C* the concentration of **1** (mM) at time *t* (min) and C_0 the initial concentration.

$$C = C_0\, e^{-kt} \tag{1}$$

Degradation rate constants under isothermal conditions were estimated using nonlinear regression. Arrhenius (eq 2) and Eyring equations (eq 3) were used to estimate the temperature (*T*) and pressure (*P*) dependence of the degradation rate constants under, respectively, isobaric and isothermal conditions, described as the activation energy (E_a, J mol^{-1}) and activation volume ($\Delta V_0^{\ddagger}$, cm^3 mol^{-1}), with R_g the universal gas constant (8.314 J mol^{-1} K^{-1}), $k_{T\mathrm{ref}}$ and $k_{P\mathrm{ref}}$ the degradation rate constants (min^{-1}) at, respectively, reference temperature T_{ref} (K) and pressure P_{ref} (MPa).

$$k = k_{T_{ref}}\, e^{-E_a\left(\frac{1}{T}-\frac{1}{T_{ref}}\right)/R_g} \tag{2}$$

$$k = k_{P_{ref}}\, e^{-\Delta V_0^{\ddagger}(P-P_{ref})/(R_g T)} \tag{3}$$

For all data analyses, aforementioned equations were assumed to be linear in the pressure−temperature range studied, implying that the change of free energy of activation of the reaction over pressure remains constant in the investigated temperature range, that is, $(d\Delta G^{\ddagger}/dP)_T$ is constant. Combined pressure−temperature dependencies of degradation rate constants were estimated on the basis of the thermodynamic model described earlier (*23*) (eq 4), which can be recalculated through the reaction Gibbs energy, ΔG (eq 5) into a kinetic thermodynamic model (eq 6), with $\Delta\beta$ and $\Delta\kappa^{\ddagger}$ representing the compressibility factor (MPa^{-1} cm^3 mol^{-1}), Δα and $\Delta\zeta^{\ddagger}$ the thermal expansibility (K^{-1} cm^3 mol^{-1}), ΔC_p and $\Delta C_p^{\ddagger}$ the heat capacity (J K^{-1} mol^{-1}), ΔV_0 and $\Delta V_0^{\ddagger}$ the activation volume (cm^3 mol^{-1}), ΔS_0 and $\Delta S_0^{\ddagger}$ the entropy change (J K^{-1} mol^{-1}) of the reaction and where ‡ represents the properties related to the activated complex.

$$\Delta G = \frac{\Delta\beta}{2T}(P-P_{ref})^2 + \Delta\alpha(P-P_{ref})(T-T_{ref}) - \Delta C_p\left[T\left(\ln\frac{T}{T_{ref}}-1\right)+T_{ref}\right] + \Delta V_0(P-P_{ref}) + \Delta S_0(T-T_{ref}) + \Delta G^0 \tag{4}$$

$$\Delta G = \Delta G^0 R_g T \ln(K^{\ddagger}) \tag{5}$$

$$\ln(k) = -\frac{\Delta\kappa^{\ddagger}}{2R_gT}(P-P_{ref})^2 - \frac{\Delta\zeta^{\ddagger}}{R_gT}(P-P_{ref})(T-T_{ref}) + \frac{\Delta C_p^{\ddagger}}{R_gT}\left[T\left(\ln\frac{T}{T_{ref}}-1\right)+T_{ref}\right] - \frac{\Delta V_0^{\ddagger}}{R_gT}(P-P_{ref}) - \frac{\Delta S_0^{\ddagger}}{R_gT}(T-T_{ref}) + \ln(k_{P\mathrm{ref},T\mathrm{ref}}) \tag{6}$$

Scheme 1

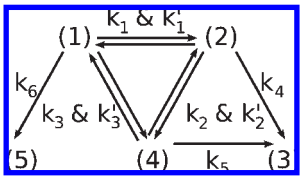

Parameters were estimated in a one-step approach by nonlinear regression analysis. Hereto, all parameter estimation and statistical data analysis was performed using the SAS v9.1.3 software package.

Calculation of Diffusion Effects. The possible impact of diffusion effects was calculated as recently described by van Boekel (*24*). Hereto, the rate constant for bimolecular encounters, k_{diff} ($dm^3\ mol^{-1}\ s^{-1}$), was determined on the basis of the Stokes−Einstein relationship, derived to eq 7, with η_v approximated by the dynamic viscosity of water ($N\ s\ m^{-2}$). For the different pressure−temperature conditions, η_v was calculated using the IAPWS-95 formulation (*25*).

$$k_{diff} = \frac{8 \times 10^3 R_g T}{3\eta_v} \quad (7)$$

To check whether or not the reactions were diffusion controlled, the reaction rate of the chemical reactions, k_{chem} ($dm^3\ mol^{-1}\ s^{-1}$), was calculated using eq 8 where the overall reaction rates, $k_{overall}$ ($dm^3\ mol^{-1}\ s^{-1}$), were derived from the k values (min^{-1}) estimated by single-response modeling.

$$\frac{1}{k_{overall}} = \frac{1}{k_{chem}} + \frac{1}{k_{diff}} \quad (8)$$

Multiresponse Kinetic Modeling. Multiresponse modeling was performed to investigate the degradation mechanism of **1**. On the basis of the current spectral data, the reaction mechanism for oxidation of **1** by O_2 or H_2O_2 at atmospheric pressure (*26*, *27*) was revised as depicted in **Figure 2**. To elucidate the exact degradation mechanism, different pathways and reversible reactions for the formation of **2**, **3**, and **4** can be considered. Additional reactions were included to account for unknown/undetected degradation products from **1**. Hereto, the four measured responses were modeled simultaneously in an iterative process by reaction models that incorporated different routes for the degradation and concomitant product formation as summarized in **Scheme 1**.

For each step in the reaction network, a differential equation was set up describing the reaction rate, for example, for the most complex reaction network in **Scheme 1**

$$\frac{d[\mathbf{1}]}{dt} = -(k_1 + k_3 + k_6)[\mathbf{1}] + k'_1[\mathbf{2}] + k'_3[\mathbf{4}] \quad (9)$$

$$\frac{d[\mathbf{2}]}{dt} = k_1[\mathbf{1}] - (k'_1 + k_2 + k_4)[\mathbf{2}] + k'_2[\mathbf{4}] \quad (10)$$

$$\frac{d[\mathbf{3}]}{dt} = k_4[\mathbf{2}] + k_5[\mathbf{4}] \quad (11)$$

$$\frac{d[\mathbf{4}]}{dt} = k_3[\mathbf{1}] + k_2[\mathbf{2}] - (k'_2 + k'_3 + k_5)[\mathbf{4}] \quad (12)$$

where [compound no.] represents the concentration of the different compounds, k the reaction rate constant, and t the reaction time under isothermal−isobaric conditions.

Under isobaric conditions, the effect of temperature on each reaction was expressed by the Arrhenius equation (eq 2). Under isothermal conditions, the effect of pressure on each reaction was expressed by the Eyring equation (eq 3). Substitution of eq 2 or 3 into the differential equations 9−12 renders the mathematical model to be solved, respectively, under isobaric and isothermal conditions using numerical integration. The corresponding kinetic parameters, the reaction rate constants, the activation energies, and the activation volumes of the various reactions were estimated simultaneously by nonlinear regression using the multiresponse Bayesian estimation software package Athena Visual Studio v12.1 (www.athenavisual.com). Conform with statistical demands for multiresponse modeling, the commonly used least-squares minimization was replaced by the determinant criterion as fit criterion (*24*). Model discrimination was based on the normalized marginal posterior probabilities for the candidate models and the lack of fit measure (*28*). Furthermore, the goodness of fit of the model was evaluated by scrutiny of the residuals.

RESULTS AND DISCUSSION

Degradation in Aqueous Solution during Thermal and HP/T Treatments. Degradation of **1** (≈0.4 μM) in water with a standardized initial oxygen concentration of 228−258 μM was studied on a kinetic basis for thermal (0.1 MPa, 40−90 °C, 2−60 min) and combined pressure−temperature treatments (100−700 MPa, 35−60 °C, 2−60 min). In accordance with previous research performed in buffer systems (*9*, *11*, *12*), degradation kinetics could be described by an apparent first-order kinetic model during isothermal−isobaric conditions in the investigated time−temperature−pressure domain (for estimated k values, see the Supporting Information). Estimated activation energies and activation volumes are presented in **Table 1**. At pressures and initial temperatures above 100 MPa and 40 °C, respectively, it was observed that both pressure and temperature increments enhanced the degradation rate of **1** (observed up to 60 min). On the basis of the estimated parameters, it was shown that under isobaric conditions k values increased with increasing temperature. In addition, the estimated negative activation volume at 40−60 °C indicated that the degradation was accelerated by application of pressure in accordance with previous results (*9*, *12*). It should be noted, however, that part of the degradation already occurred during the dynamic pressure−temperature phase due to pressure buildup. In this context, losses of 5−40% of **1** were observed in the blanks (t_0) relative to the untreated samples. Presumably this effect is attributed to the inherent temperature increment of 0.03 °C MPa^{-1} during adiabatic heating. To date, however, these dynamic pressure−temperature conditions cannot be accounted for in the description of folate degradation kinetics.

The estimated E_a values (**Table 1**) at different pressure levels were lower than previously reported in, for example, phosphate buffer systems (*9*, *11*, *12*). This incoherence could be caused by the presence of buffer ions, trace metals, or β-mercaptoethanol and/or by pressure-dependent pH changes in the model systems used (*11*, *29*, *30*), which were neglected in the previous investigations. In addition, the activation energy is a very complicated quantity in solutions that depends on the energy of the entire local assembly of reactants and solvent molecules (e.g., diffusion effects). It should be noted that the calculated dynamic viscosity of water increases by ±35% at 60 °C from 0.1 to 500 MPa and that higher viscosities are expected within the investigated temperature−pressure region up to 700 MPa (*25*). It is hence plausible that the temperature dependency of the elementary reaction rate constants is not linear over the investigated pressure−temperature domain as assumed in eq 2. This effect would largely depend on the occurrence of activation- and diffusion-controlled reactions in the degradation mechanism. Calculations of the impact of diffusion effects showed that k_{diff} ranged from 8.14×10^9 to 2.56×10^{10} $dm^3\ mol^{-1}\ s^{-1}$. As depicted in **Figure 3**, diffusion was not rate limiting up to 500 MPa and, hence, it can be stated that the degradation of **1** is activation-controlled.

Because it was previously reported that the overall degradation of **1** slows down at atmospheric pressure from pH 5.6 to 4 [i.e., the region in which N(5) becomes protonated] in aqueous solution (*27*) and because water shows a pH shift toward lower values over the investigated pressure−temperature conditions

Table 1. Estimated Temperature (E_a Values, T_{ref} = 50 °C), Pressure ($\Delta V_0^{\ddagger}$ Values, P_{ref} = 400 MPa) and Combined Pressure−Temperature Dependence (T_{ref} = 50, P_{ref} = 400 MPa) for [6*S*]5-Methyltetrahydrofolic Acid Degradation (≈0.4 μM) in Water during Thermal (0.1 MPa, 40−90 °C, 2−60 min) and HP/T (100−700 MPa, 35−60, 2−60 min) Treatments[a]

temperature dependence			pressure dependence		
pressure (MPa)	E_a (kJ mol^{-1})	*P*	temperature (°C)	$\Delta V_0^{\ddagger}$ (cm^3 mol^{-1})	*P*
0.1	73.1 ± 3.6	<0.0001	40	−6.4 ± 1.1	<0.0001
200	53.8 ± 7.9	<0.0001	45	−4.1 ± 0.7	<0.0001
300	58.4 ± 13.4	0.0003	50	−4.1 ± 0.4	<0.0001
400	66.8 ± 6.5	<0.0001	60	−3.3 ± 0.9	0.0008
500	85.2 ± 4.4	<0.0001			
600	32.4 ± 8.4	<0.0001			
700	27.1 ± 5.9	<0.0001			

Combined Pressure−Temperature Dependence

thermodynamic model			empiric model		
parameter	estimate	*P*	parameter	estimate	*P*
$\Delta\kappa^{\ddagger}$(MPa^{-1}cm^3 mol^{-1})	0.002 ± 0.014	0.8875	*A* (K MPa^{-1})	0.58 ± 0.14	0.0005
$\Delta V_0^{\ddagger}$ (cm^3 mol^{-1})	−3.97 ± 1.26	0.0068	*B*	27.1 ± 3.5	<0.0001
$\Delta S_0^{\ddagger}$ (J K^{-1} mol^1)	138.8 ± 28.9	0.0002	$k_{Pref,Tref}$ (min^{-1})	0.027 ± 0.002	<0.0001
$\Delta\zeta^{\ddagger}$ (K^{-1} cm^3 mol^{-1})	−0.28 ± 0.19	0.1489	corrected R^2	0.96	
$\Delta C_p^{\ddagger}$ (J K^{-1} mol^{-1})	5203 ± 2417	0.0481	SD	0.0086	
$k_{Pref,Tref}$ (min^{-1})	0.026 ± 0.003	<0.0001			

[a] Values are presented ±95% HPD interval and parameter significance. For empiric model parameters, corrected R^2 and standard deviation (SD) of the nonlinear regression model, using eq 13, are presented.

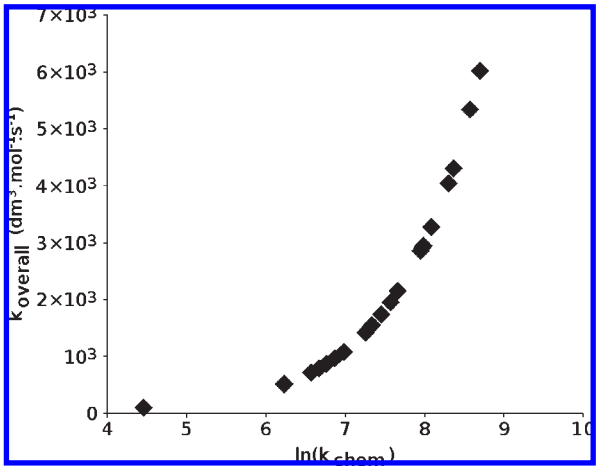

Figure 3. Estimated overall reaction rate constants, $k_{overall}$ (dm^3 mol^{-1} s^{-1}), as a function of the corresponding chemical rate constants, k_{chem} (dm^3 mol^{-1} s^{-1}), calculated using eqs 7 and 8.

(see Supporting Information) (*39*), it could be considered as another factor that could influence the degradation of **1**. The current results, however, showed that the degradation of **1** was accelerated and not decelerated with increasing pressure and/or temperature. Therefore, it was expected that the effect of pressure and/or temperature was more important than the shift in pH under the investigated conditions.

Little is known concerning the mechanistic background of degradation of **1** under pressure. In this context, HP/T degradation of **1** was previously hypothesized to be caused by oxidative degradation with subsequent cleavage of the C(9)−N(10) bond and was approximated as a single-step reaction (*9*). To describe the combined pressure−temperature dependency of folate degradation reactions, thermodynamic (eq 6) and derived empirical kinetic models were used in preceding research (*9*, *10*, *12*). Based on activated complex theory and developed to describe pressure−temperature inactivation of enzymes (*23*), the aforementioned models imply that all degradation reactions are reduced to a single transition state system. As a consequence, this allowed prediction of the combined pressure−temperature dependency of apparent first-order degradation rate constants by kinetic models solely based on measurements of residual (nondegraded) folate concentrations without any mechanistic insight.

Fitting the thermodynamic model (eq 4) in a similar approach to the present data showed that thermal expansibility ($\zeta^{\ddagger}$), compressibility ($\Delta\kappa^{\ddagger}$), and heat capacity ($\Delta C_p^{\ddagger}$) were nonsignificant parameters ($P > 0.01$, **Table 1**). It was described earlier (*12*) that omittance of these parameters implies independence of the activation volume from pressure and temperature and, consequently, loss of the model's thermodynamic signification. The resulting empirical kinetic model with significant empiric parameters *A* (K MPa^{-1}) and *B* (dimensionless) is described in eq 13, and the estimated parameters are presented in **Table 1**.

$$k_{P,T} = k_{P_{ref},T_{ref}}\, e^{A(P-P_{ref})/T}\, e^{B(T-T_{ref})/T} \qquad (13)$$

Scrutiny of the residuals revealed that the model adequately fits the experimental data.

Identification of Degradation Products. To screen breakdown products formed during processing, **1** (≈40 μM) was subjected to thermal (0.1 MPa, 60−100 °C, 2−60 min) and HP/T treatments (200−800 MPa, 50−65 °C, 2−40 min) and analyzed by HPLC-UV-DAD and ESI-MS. The presence of **1** in untreated samples was validated on the basis of its characteristic UV spectrum (**Figure 4**) and the CID fragmentation pattern of the protonated molecular ion (*m*/*e* 460.3) at 25% source energy: 180.2 (9), 181.2 (4), 313.2 (100), 331.1 (18), 345.1 (27), 442.1 (1). The three intense fragmentation losses conform with literature data (*31*−*33*). Upon heating or HP/T treatment, formation of several unknown degradation products was observed by HPLC using DAD detection at 210−400 nm. Occurrence of **2** and **3** in the degradation solutions was corroborated by comparison of retention times and UV spectra with external standards. Furthermore, LC-MS analysis of HP/T and thermally treated samples indicated that a component with a protonated molecular ion *m*/*e* 474.3 was formed as predominant degradation product in the initial stages under the investigated conditions. Structural information of this

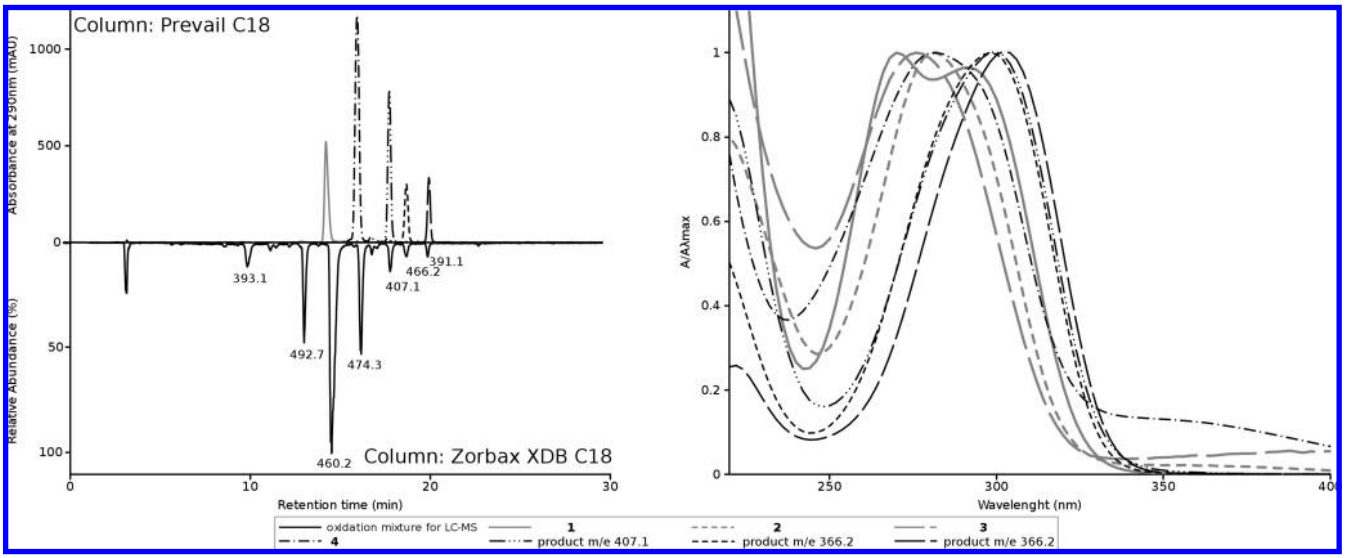

Figure 4. (Left) Overlay of UV-DAD chromatograms of **1**and its purified degradation products after heating at 100 °C for 24 h in water. The corresponding LC-MS chromatogram with predominant *m/e* values in the detected peaks of the degradation mixture is mirrored as reference. (Right) Overlay of UV-DAD spectra of **1** and its purified degradation products.

degradation product was obtained by its CID fragmentation pattern at 25% CID energy: *m/e* 326.7 (3), 345.1 (100), 359.0 (14), 456.1 (46). Comparison with the CID fragmentation pattern of **1** suggested the loss of two hydrogen atoms and the addition of an oxygen atom in the pteridine part of the molecule. For the parent ion at *m/e* 474.3, the fragment ion at *m/e* 345.1 indicated a loss of 129 mass units due to cleavage between N(18) and C(19) in glutamic acid, whereas the ion at *m/e* 326.7 represents the neutral loss of the glutamate moiety. Previously, oxidation of **1** with H_2O_2 at pH 6 for 1 h at room temperature has been shown to produce 2-amino-8-methyl-4,9-dioxo-7-methyl-*p*-aminobenzoylglutamate-6,7,8,9-tetrahydro-4*H*-pyrazino(1,2-*a*)-*s*-triazine (**4**; **Figure 1**) as peroxidation product (*34*). Because the latter may occur as a protonated molecular ion approximately at *m/e* 474, this was a plausible candidate for the structure of the degradation product under the investigated conditions. It should be noted, however, that the majority of the aforementioned CID cleavages were due to losses and rearrangements on the glutamyl part of the molecule. As a consequence, it was deemed to be too tentative to draw conclusions regarding the exact structure of the pteridine part in the degradation product based solely on the MS data. Hereto, acquisition of spectral information by NMR measurements was deemed to be necessary.

To identify the aforementioned component, an aqueous solution of **1** (≈4 mM) was heated for 24 h at 100 °C, and subsequently degradation products were purified by semipreparative HPLC. Despite the prolonged heating period, **1** was still present in the degradation solution, whereas **2** was not detected by LC-MS. Because **1** occurred in excess relative to the initial O_2 concentration (0.26 mM), **1** was stable after consumption of molecular O_2 in accordance with previous results (*20*). Besides **1** and the component with *m/e* 474.3 (**4**), novel degradation products with *m/e* 393.3, 492.7, 407.1, 466.2, and 391.2 were detected by LC-MS (**Figure 4**).

After purification and lyophilization, a small yield of **1** and four other products was obtained. **4** Occurred as a bright yellow powder, whereas other products occurred as white powders. Further analysis showed that the absorption maximum at 270 ± 2 nm in the UV spectrum of **1** disappeared in the degradation products under the chromatographic conditions. Concurrent to this, a small bathochromic shift (6−12 nm) of the second absorbance maximum at 289 ± 2 nm occurred for most products (**Figure 4**).

Detailed clarification of the molecular structure of **4** was performed on the basis of spectral analyses at 600 MHz in $^2H_6$-DMSO and expressed relative to $(CH_3)_4Si$ (see the Supporting Information). The ^1H and ^{13}C NMR spectra of the purified free acid of **1** were very similar to the spectra in ^2H_2O reported by others (*34*, *35*) and were hence used as reference. The purified degradation product was identified as 2-amino-8-methyl-4,9-dioxo-7-methyl-*p*-aminobenzoylglutamate-6,7,8,9-tetrahydro-4*H*-pyrazino(1,2-*a*)-*s*-triazine (**4**; **Figure 1**). Comparison of NMR spectra with **1** showed that the characteristic ^1H NMR signals of the *p*-aminobenzoyl-L-glutamic acid moiety were retained in the oxidation product, whereas signals for H_2−C(9), H−C(6), and H_2−C(7) in **1** were replaced by several downfield signals in the degradation product. Moreover, the characteristic singlet at 2.49 ppm of the N(5)−C(5α)H_3 in **1** was shifted downfield to 3.06 ppm, and this methyl group caused a signal in the HMBC NMR spectrum that correlated respectively with the C(9) carbonyl group and with the C(7) methine group in the oxidation product (see the Supporting Information). In addition, occurrence of the H−C(5) protons in **4** as a dd at 3.77 ppm and as a brd d at 4.38 ppm indicated in combination with the HSQC NMR measurements the occurrence of H_S−C(6) and H_R−C(6) protons with a spin−spin coupling constant of $J = 14.04$ Hz, typical for a geminally coupled axial−equatorial proton pair on a carbon in a six-membered ring. In accordance with other spectral observations (*34*) the C(4a) signal at 100.39 ppm from **1** had dissapeared in the degradation product and a new signal was observed in the carbonyl region of the spectrum at 155.71 ppm. In accordance with the structure proposed in the aforementioned report (*34*), this suggested that the C(4a) from **1** is converted to a carbonyl group in the oxidation process with a subsequent rearrangement of the pteridine nucleus to an *s*-triazine derivative. Regarding the other degradation products, however, spectral analysis was not possible because purification yields were too low, and hence further identification of these intermediates based solely on the MS data was deemed to be too tentative.

On the basis of the current results and in accordance with the proposed oxidation mechanism of **1** by O_2 or H_2O_2 at atmospheric pressure (*26*, *27*, *34*), it could be suggested that the

formation of **4** could occur from **1** and/or **2** during thermal and HP/T treatments in one of the mechanisms described in **Scheme 1**. The finding of **3** as a degradation product could be attributed to hydrolysis of the C(9)−N(10) covalent bond in **1** or the C(11)−N(12) bond in **4**, in analogy with C(9)−N(10) bond cleavage shown for folic acid (*36*).

Degradation Mechanism in Aqueous Solution during Thermal Treatments. To elucidate the degradation mechanism of **1** and to validate the estimated kinetic parameters obtained earlier by single-response modeling, multiresponse modeling was applied. Multiresponse modeling implies that besides **1**, more responses are simultaneously taken into account and that the measured responses have one or more parameters in common. The multiresponse approach provides an advantage over single-response modeling by obtaining more precise parameter estimates and by gaining more in-depth insights of the underlying reaction mechanism using model discrimination. In this context, each kinetic model is proposed on the basis of a postulated reaction mechanism, and the related models are subsequently fit to the experimental data using the determinant criterion (*24*). For each model a goodness of fit measure indicates the consistency between the data and the postulated model (*28*). If the goodness of fit is inadequate, the assumed model is incorrect and should be refined. In an iterative process the fitting procedure is repeated until the best acceptable model is found, that is, the model with the largest posterior probability share in the model candidate set (*28*).

In the current investigation, concentrations of **1**, **2**, **3**, and **4** were quantifiable in thermally treated samples (0.1 MPa, 60−100 °C, 0−60 min) with initial folate and O_2 concentrations of, respectively, 0.04 and 0.26 mM. It was observed that the concentration of **1** decreased with treatment time upon heating of the solutions, whereas concentrations of **2** and **4** increased. At temperatures above 90 °C and heating times above 10 min, decreases in **2** and **4** coincided with detectable formation of **3**, which was not observed for the milder conditions (**Figure 6**). As expected, the rate of loss of **1** and the rate of formation of **2** and **4** increased with increasing treatment temperature.

To model the reactions taking place in the model systems at atmospheric pressure, a kinetic model was constructed starting from the autoxidation mechanism originally proposed by Blair and co-workers (*27*). The mechanism assumes that **1** reacts with molecular O_2 in solution to form a hydroperoxyl radical as chain carrier and an intermediate trihydropteridine radical with the unpaired electron situated on N(5) or C(4a) (*37*). It was previously considered that the trihydropteridine radical subsequently reacts to a quinoid 6,7-dihydropteridine that can either undergo (i) rearrangement to **2** or (ii) covalent hydration to form a stable (4a) hydroxy-6,7-dihydropteridine (*26*, *27*, *37*). Instead of a (4a) hydroxy-6,7-dihydropteridine, **4** was detected as main oxidation product of **1** in the current investigation and is supported by later NMR observations alluding to the occurrence of a rearrangement reaction in the pteridine nucleus (*34*). On the basis of the recent proof of superoxide anion formation during autoxidation of tetrahydropterin with molecular oxygen (*38*), it is suggested that the formation of **4** could hence occur as depicted in **Figure 5** via a trihydropteridine radical (**1.a**) and quinoid 6,7-dihydropteridine (**1.b**). Subsequent formation of an isocyanate (**1.c**) that reacts to a hydroperoxide (**1.d**) could result in the formation of **4** upon loss of water. It should be noted that the formation of **1.d** was supported by the detection of a component with *m*/*e* 492.7 during the MS experiments. However, no spectral analysis of this molecule was possible, and hence further validation is needed for this hypothesis.

To corroborate the proposed degradation mechanism with the experimental data, the reaction model from **Figure 2** was refined in an iterative procedure by simultaneously fitting different reaction models incorporating different possible formation routes of **3** and **4**. On the basis of the normalized marginal posterior probability share of the different kinetic models, the mechanism described in **Scheme 2** resulted in the most accurate fit for the data.

Predicted and experimental concentrations of the measured responses per temperature (60−100 °C) as a function of treatment time for this model plus normal probability plots used to assess the model fit are presented in **Figure 6**.

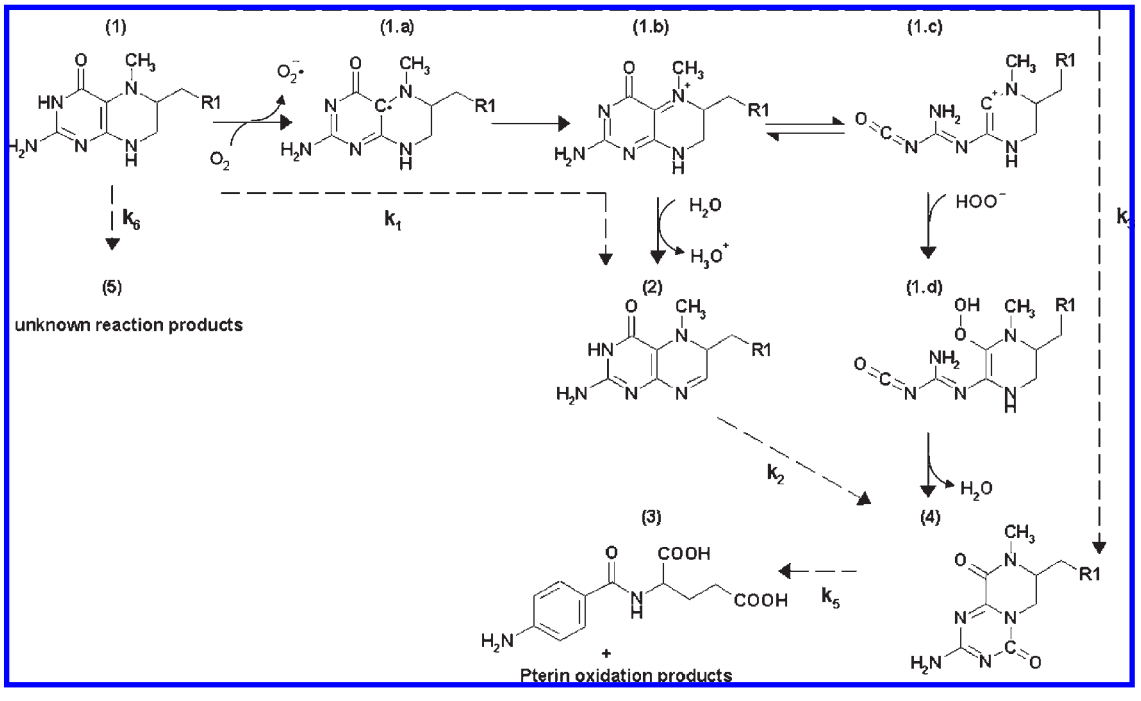

Figure 5. Degradation mechanism of **1** during thermal and HP/T treatments based on the current spectral data and multiresponse modeling. R_1 represents the *p*-aminobenzoyl-L-glutamate part of the molecules.

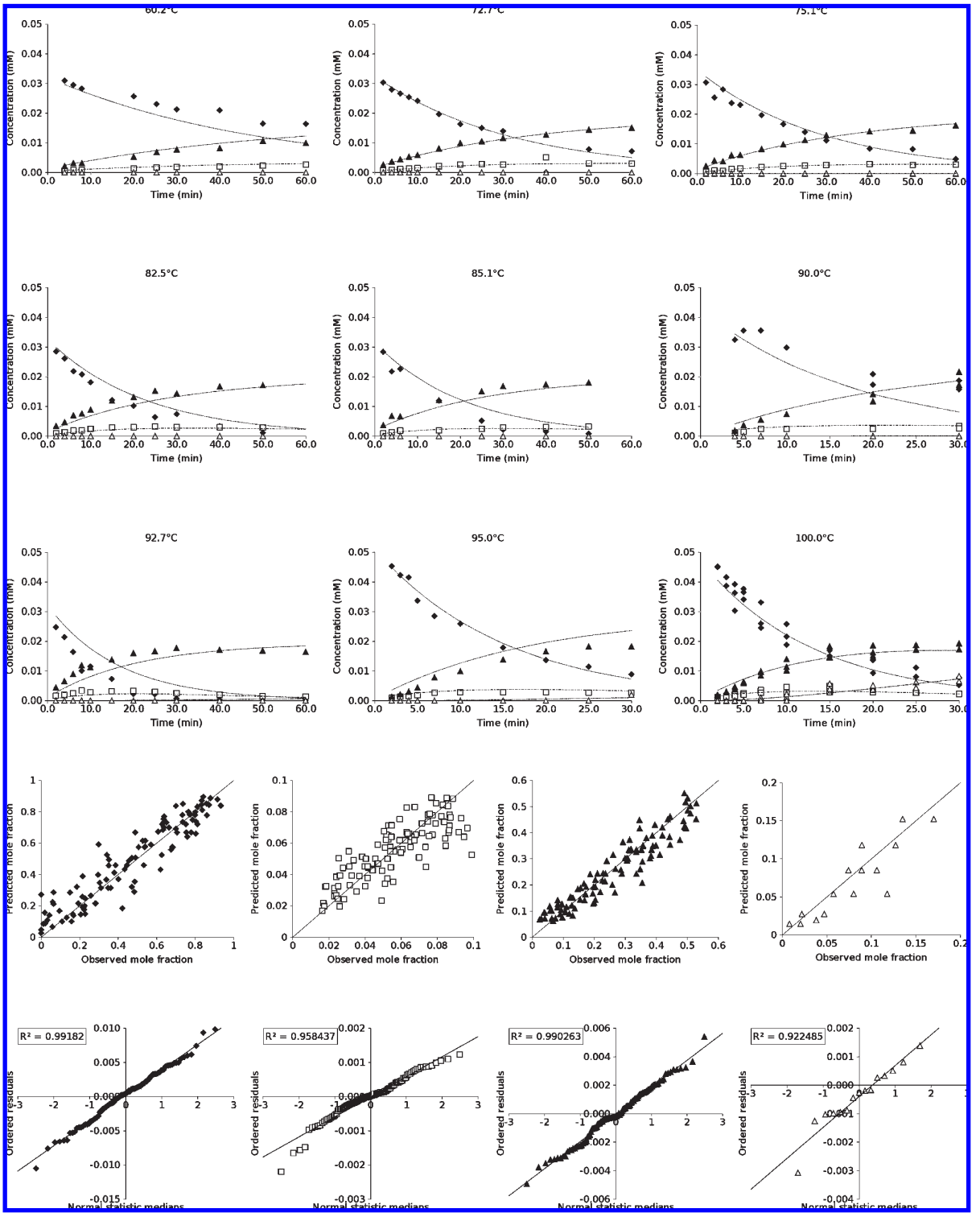

Figure 6. Time course for degradation of **1** (◆, ≈0.04 mM) and formation of **2** (△), **3** (□), and **4** (▲) in water heated at 60−100 °C at atmospheric pressure. Lines represent the model fit using the Arrhenius equation. Parity and normal probability plots for model fit assessment are presented in the last two rows, where solid lines represent an ideal fit.

An accurate model fit was obtained for **1**, **2**, **3**, and **4** under most conditions as confirmed in the parity plots. In addition, no trend was observed within the residuals, and on the basis of the normalized parameter covariance matrix, none of the parameters were highly correlated to each other. The estimated parameters, that is, the k_{ref} and E_a values, corresponding to the "elementary" reactions in **Scheme 2**, are listed with their 95% highest posterior density (HPD) confidence interval in **Table 2**. The results imply that **2** and **4** can be formed directly from **1** and that **4** can also be formed from **2**. In accordance with **Figure 5** and with the previously postulated route for the formation of **2** from **1** (*27*), these results indicate a reversible rearrangement reaction from **1.b** to **2**. In addition, **1** undergoes further degradation for which the responses were not measured. According to the modeled mechanism, the formation of **2** from **1** at atmospheric pressure is a relatively slow reaction in comparison to the formation of **4** and other degradation products from **1**. Moreover, **2** reacts rapidly to **4**, which slowly undergoes further degradation to **3** and pteridine

oxidation products. Unexpectedly, no formation of **3** from **2** could be modeled for the current data. This reaction was previously shown to occur in folic acid through participation of freely diffusible superoxide anion and hydroxyl radicals in the hydrolysis of the C(9)−N(10) covalent bond via a hydrogen atom transport mechanism with the formation of a C(9)-centered radical as intermediate (*36*). The current observation could hence indicate that the electron-donating N(5) methyl group would stabilize the N(10) secondary amine in **2**. In accordance with the current results, C(11)−N(12) bond cleavage could be possible in **4** because the aforementioned effect would be restricted by the adjacent carbonyl group on C(9) in the rearranged pteridine nucleus.

Degradation Mechanism in Aqueous Solution during HP/T Treatments. The impact of elevated pressure on the degradation pathways of **1** (0.04 mM) was studied on a multiresponse kinetic basis at 800 MPa and 50−65 °C (0−33 min) and at 200−800 MPa and 60 °C (0−33 min). On the basis of the chromatograms, formation of **2**, **4**, and **3** was confirmed to occur under the investigated conditions (**Figure 7**). Formation of **3** was not expected to take place to the observed extent at 800 MPa because homolytic cleavage of the secondary amine covalent bond should be characterized by an activation volume ($\Delta V_0^{\ddagger}$) around 10 cm^3 mol^{-1} (*4*,*21*) and hence be retarded by the application of pressure. In addition, peaks that were only minimally detected in samples treated at atmospheric pressure appeared in the chromatograms of the pressure-treated samples.

Because pressure changes cannot be the cause of entirely new reaction mechanisms (*21*), accumulation of **3** and the unknown products suggested that the related degradation reactions in **Figure 5** (i.e., **1** → **5** and **4** → **3**) are characterized by a negative $\Delta V_0^{\ddagger}$ and hence favored over other reaction pathways under pressure. The validity of the proposed degradation mechanism at atmospheric pressure was therefore investigated under isothermal conditions (60 °C) at different pressures (200−800 MPa) by fitting the reaction model (**Scheme 2**) onto the measured responses using the Eyring equation (eq 3). This description of the pressure dependence of the reaction rate constants clearly indicated that the formation of **4** directly from **1** was retarded at 60 °C and characterized by a large positive $\Delta V_0^{\ddagger}$ (**Table 2**). As a consequence, the corresponding k value at reference pressure 400 MPa was too low to be estimated in a single step with the other parameters and was estimated as $(3.5 \pm 0.9) \times 10^{-5}$ min^{-1} when all other parameters were considered to be fixed values. It should be noted that the estimated $\Delta V_0^{\ddagger}$ for this reaction is in accordance with the neutralization of charges in the proposed rearrangement mechanism depicted in **Figure 5**. Neutralization would be expected to cause solvent relaxation and hence expansion even if bond formation would take place simultaneously (*21*). In contrast to the aforementioned reaction, most other degradation reactions were accelerated with increasing pressure and characterized by negative $\Delta V_0^{\ddagger}$ values ranging between −3.2 and −15.4 cm^3 min^{-1} (**Table 2**).

Estimation of the temperature dependence of the degradation rate constants at 800 MPa was performed by fitting the reaction model onto the responses measured at 50−65 °C per pressure−temperature combination. In accordance with its previously estimated $\Delta V_0^{\ddagger}$ at 60 °C, results showed that no significant k values could be estimated for the formation of **4** from **1** under the investigated conditions. Plotting the estimated ln(k) values for the other reactions against the inverse temperature indicated that these reactions exhibited Arrhenius behavior at 800 MPa. Most of **1** had, however, already been oxidized during the dynamic pressure buildup phase to reach isobaric−isothermal conditions at 800 MPa and 65 °C, and due to the concurrent acceleration of the side reactions no reaction rate constant could be estimated for the formation of **2** from **1** under those conditions. As a consequence, the corresponding activation energy could not be precisely estimated when the reaction model was fit onto all measured responses at 50−65 °C using eq 2. Estimated E_a values are shown in **Table 2**. In contrast to the other reactions, a negative activation energy was observed for the formation of **3** from **4**, implying that the reaction rate decreased with increasing

Scheme 2

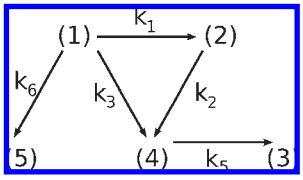

Table 2. Estimated k_{ref} ($\times 10^{-3}$ min^{-1}), E_a (kJ mol^{-1}), $\Delta V_0^{\ddagger}$ (cm^3 mol^{-1}), and Empiric Model Parameters [A ($KMPa^{-1}$) and B in Equation 13] for [6*S*]5-Methyltetrahydrofolic Acid (≈0.04 mM) Degradation Reactions in Water during, Respectively, Thermal (0.1 MPa, 60−100 °C, 0−60 min) and HP/T Treatments (200−800 MPa, 50−65 °C, 0−40 min) According to the Reaction Model in **Scheme 2**[a]

	temperature dependence		pressure dependence		temperature dependence	
	0.1 MPa, 60−100 °C		200−800 MPa, 60 °C		800 MPa, 50−65 °C	
reaction	k_{Tref}[b]	E_a	k_{Pref}[c]	$\Delta V_0^{\ddagger}$	k_{Tref}[d]	E_a
1 → 2	9.43 ± 0.82	37.8 ± 6.4	38.1 ± 5.8	−3.7 ± 1.9	16.0 ± 6.5	−20.7 ± 72.1
2 → 4	41.2 ± 5.3	79 ± 12	25.8 ± 0.5	−3.2 ± 1.7	27.4 ± 5.1	55.6 ± 28.6
1 → 4	29.6 ± 2.0	33.4 ± 5.2	indeterminate		indeterminate	
4 → 3	2.26 ± 0.98	490 ± 100	1.6 ± 0.4	−5.7 ± 1.8	6.5 ± 0.7	−56.4 ± 18.6
1 → 5	25.8 ± 2.5	35.4 ± 8.5	45.0 ± 15.0	−15.4 ± 4.0	53.2 ± 6.8	84.1 ± 26.0

	Combined Pressure−Temperature Dependence		
	600−800 MPa, 50−65 °C		
reaction	$k_{Tref,Tref}$[e]	A	B
1 → 2	0.021 ± 0.011	−0.13 ± 0.34	16.4 ± 19.2
2 → 4	0.017 ± 0.007	0.16 ± 0.19	24.0 ± 12.4
1 → 4	indeterminate	indeterminate	indeterminate
4 → 3	0.008 ± 0.004	0.78 ± 0.36	−22.7 ± 84
1 → 5	0.007 ± 0.003	1.11 ± 0.37	48.6 ± 14.9

[a] Values are presented ±95% HPD interval. [b] T_{ref} = 95 °C. [c] P_{ref} = 400 MPa. [d] T_{ref} = 55 °C. [e] T_{ref} = 50 °C, P_{ref} = 400 MPa.

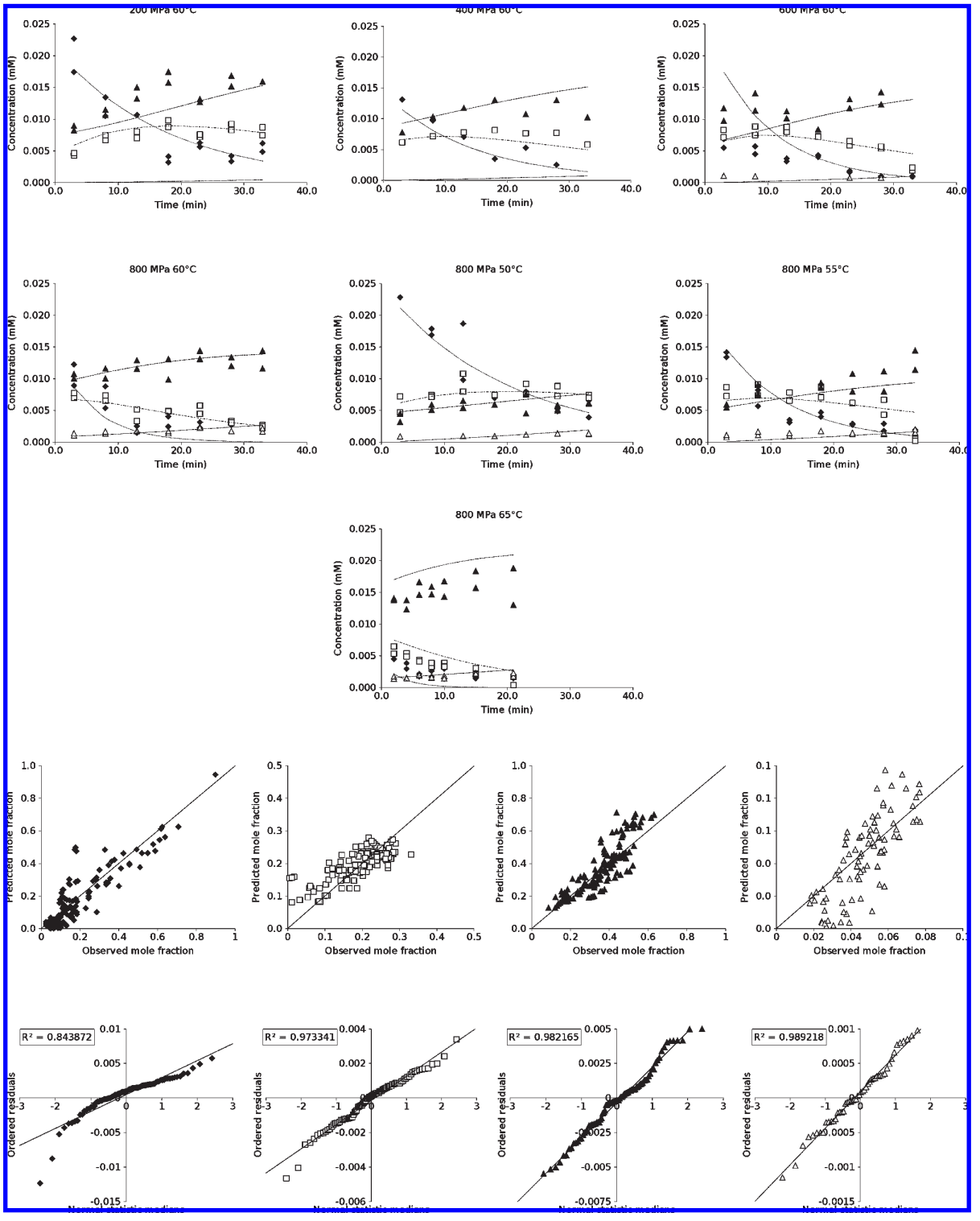

Figure 7. Time course for degradation of **1** (◆, ≈0.04 mM) and formation of **2** (△), **3** (□), and **4** (▲) in water during HP/T treatments (200−800 MPa, 50−65 °C, 0−33 min). Lines represent the model fit using the empiric model for combined pressure−temperature dependence of *k* values (eq 13). Parity and normal probability plots for model fit assessment are presented in the last two rows, where solid lines represent an ideal fit.

temperature. This suggests that the corresponding reverse reaction which results in depletion of the activated complex formed during the hydrogen atom transport mechanism of the C(11)−N(12) bond cleavage is so sensitive to temperature at 800 MPa that its rate sharply rises with increasing temperature.

To validate the empiric model obtained earlier by single-response modeling, eq 13 was used in a multiresponse modeling approach to describe the combined pressure and temperature dependence of the degradation rate constants in the reaction model (**Scheme 2**) for all responses (200−800 MPa, 50−65 °C, 0−33 min) simultaneously. In accordance with the previous multiresponse results, no parameters could be estimated for the direct formation of **4** from **1**. All other degradation reactions were adequately modeled by the empiric model for most of the investigated conditions as depicted in **Figure 7**. The estimated parameters are shown in **Table 2**. Parity and normal probability

plots used to assess the model fit are also presented in **Figure 7** and indicated, besides the model accuracy for most responses, that no trend was observed within the residuals. Moreover, none of the parameters were highly correlated to each other on the basis of the normalized parameter covariance matrix. As depicted in **Figure 7**, concentrations of **4** were underestimated at 60 and 200 MPa, indicating that the reaction **1** → **4** still occurred at a significant rate under those conditions. Under the most extreme conditions (i.e., 65 °C, 800 MPa), concentrations of **1** were underestimated by the model, whereas concentrations of **2** and **4** were clearly overestimated. This lack of fit indicated a failure of the model. As stated earlier, it is plausible that the degradation was slowed at 65 °C and 800 MPa because the pH under those conditions could have induced protonation of N(5) in **1**. The resulting goodness of fit for the total data set, however, was quite satisfactory, and on the basis of the replicate experiments, the model remained statistically acceptable to describe the different responses measured. In conclusion, it should be considered that this does not mean that the kinetic model represents the exact reaction mechanisms, but it indicates that the proposed reaction model is suitable to explain the experimental data. Description of the degradation via all intermediates would have been more correct in this context, but no quantitative information about these postulated products (**1.a**−**1.d**) was available. Further clarification of the degradation mechanism under pressure with concurrent estimation of the corresponding parameters and the impact of pH at the more acidic conditions (e.g., by a pH rate profile plot) was, therefore, not possible on the basis of the current data set and requires further investigation.

So far, knowledge of the chemical mechanisms and the kinetics governing the degradation of most micronutrients under pressure remain unknown but are greatly needed for high-pressure process optimization (*12*). To our knowledge, this is the first investigation in which micronutrient degradation has been studied in detail during HP/T treatments on both mechanistic and kinetic bases. Besides obtaining information on the degradation of the product of interest in accordance with previous research (*9*−*12*, *20*), valuable new information was gained regarding the formation of degradation products (i.e., **2**, **3**, and **4**) and side reactions by application of multiresponse modeling. As a consequence, this approach proves to be a promising tool to assess the impact of HP/T and other processing techniques on other nutrients and components for which chemical reactions may play an important role in the degradation. Furthermore, incorporation of fundamental mechanistic insights enables a more detailed prediction of the ongoing processes during the treatments and enhances the possibilities for process design and optimization. Thus, the limitations and incoherence among the results regarding nutrient degradation due to HP/T treatments obtained by single-response modeling in previous research may be overcome in the future. The current results suggest that reactions for degradation of **1** under pressure follow the same mechanistic pathways as observed at atmospheric pressure in the context that the elementary rate constants change according to the related activation volumes. In this context it was observed that several of the elementary reactions were characterized by a negative activation volume under HP/T conditions at 60 °C. As a consequence, the total degradation of **1** was accelerated by application of pressure in accordance with the literature. It was, however, shown that the formation of **4** directly from **1** was strongly retarded under pressure. As compared to the reactions at atmospheric pressure, high-pressure processing can result in different relative concentrations of the degradation products depending on the activation volumes of the elementary reactions.

In general, the course of the degradation reactions of **1** and its concomitant degradation products could adequately be predicted for both thermal treatments at atmospheric pressure and combined high hydrostatic pressure treatments. As suggested earlier (*12*), the current information could be used as a fundamental basis to set up a valid general kinetic model to describe the combined pressure−temperature dependence of the reaction rate constants for **1** degradation under the form of eq 13 but now for elementary degradation reactions. Further investigations in this area are still greatly needed because knowledge of the reactions that food components undergo under HP/T conditions is limited.

ACKNOWLEDGMENT

The generous gift of [6*S*]5-methyltetrahydrofolate (Metafolin) from Merck Eprova AG and the excellent technical support of K. Duerinckx for NMR measurements are gratefully acknowledged.

Supporting Information Available: Tables of first-order reaction rate constants for **1**, ^{1}H and ^{13}C signals for **4** by HSQC and by HMBC, APT, and HSQC, and pH values of water under experimental conditions. This material is available free of charge via the Internet at http://pubs.acs.org.

LITERATURE CITED

(1) Cheftel, C. Review: High pressure, microbial inactivation and food preservation. *Food Sci. Technol. Int*. **1995**, *1*, 75–90.
(2) Hayashi, R. Applications of high pressure to food processing and preservation. In *Engineering and Food*; Spiess, W., Schubert, H., Eds.; Elsevier Applied Science: London, U.K., 1989; pp 815−826.
(3) Balny, C.; Mozhaev, V.; Lange, R. Hydrostatic pressure and proteins: Basic concepts and new data. *Comp. Biochem. Physiol.* **1997**, *116A*, 299–304.
(4) Tauscher, B. Pasteurization of food by hydrostatic high-pressure—chemical aspects. *Eur. Food Res. Technol*. **1995**, *200*, 3–13.
(5) Donsi, G.; Ferrari, C.; di Matteo, M. High pressure stabilization of orange juice: evaluation of the effects of process conditions. *Ital. J. Food Sci.* **1996**, *2*, 99–106.
(6) Sancho, F.; Lambert, Y.; Demazeau, G.; Largeteau, A.; Bouvier, J.; Narbonne, J. Effect of ultra-high hydrostatic pressure on hydrosoluble vitamins. *J. Food Eng*. **1999**, *39*, 247–253.
(7) Fernandez Garcia, A.; Butz, P.; Bognar, A.; Tauscher, B. Antioxidative capacity, nutrient content and sensory quality of orange juice and an orange−lemon−carrot juice product after high pressure treatment and storage in different packaging. *Eur. Food Res. Technol*. **2001**, *213*, 290–296.
(8) Butz, P.; Serfert, Y.; Fernandez, G.; Dieterich, S.; Lindauer, R.; Bognar, A.; Tauscher, B. Influence of high-pressure yreatment at 25 and 80 °C on folates in orange juice and model media. *J. Food Sci.* **2004**, *69*, S117–S121.
(9) Nguyen, M. T.; Indrawati; Hendrickx, M. Model studies on the stability of folic acid and 5-methyltetrahydrofolic acid degradation during thermal treatment in combination with high hydrostatic pressure. *J. Agric. Food Chem*. **2003**, *51*, 3352–3357.
(10) Nguyen, M. T.; Oey, I.; Hendrickx, M.; Van Loey, A. Kinetics of (6*R*,*S*) 5-formyltetrahydrofolic acid: isobaric−isothermal degradation in a model system. *Eur. Food Res. Technol*. **2006**, *223*, 325–332.
(11) Indrawati, I.; Arroqui, C.; Messagie, I.; Nguyen, M.; Van Loey, A.; Hendrickx, M. Comparative study on pressure and temperature stability of 5-methyltetrahydrofolic acid in model systems and in food products. *J. Agric. Food Chem*. **2004**, *52*, 485–492.
(12) Indrawati; Van Loey, A.; Hendrickx, M. Pressure and temperature stability of 5-methyltetrahydrofolic acid: a kinetic study. *J. Agric. Food Chem*. **2005**, *53*, 3081–3087.
(13) Verlinde, P.; Oey, I.; Hendrickx, M.; Van Loey, A. High-pressure treatments induce folate polyglutamate profile changes in intact broccoli (*Brassica oleraceae* L. cv. Italica) tissue. *Food Chem*. **2008**, *111*, 220–229.

(14) Tamura, T.; Picciano, M. F. Folate and human reproduction. *Am. J. Clin. Nutr.* **2006**, *83*, 993–1016.
(15) Moat, S.; Lang, D.; McDowell, I.; Clarke, Z.; Madhavan, A.; Lewis, M.; Goodfellow, J. Folate, homocysteine, endothelial function and cardiovascular disease. *J. Nutr. Biochem.* **2004**, *15*, 64–79.
(16) Selhub, J.; Bagley, L.; Miller, J.; Rosenberg, I. B vitamins, homocysteine, and neurocognitive function in the elderly. *Am. J. Clin. Nutr.* **2000**, *71*, 614S–620S.
(17) Kim, Y. I. Folate and colorectal cancer: an evidence-based critical review. *Mol. Nutr. Food Res.* **2007**, *51*, 267–292.
(18) Murphy, M.; Keating, M.; Boyle, P.; Weir, D. G.; Scott, J. M. The elucidation of the mechanism of folate catabolism in the rat. *Biochem. Biophys. Res. Commun.* **1976**, *71*, 1017–1024.
(19) McKillop, D.; Pentieva, K.; Daly, D.; McPartlin, J.; Hughes, J.; Strain, J.; Scott, J.; McNulty, H. The effect of different cooking methods on folate retention in various foods that are amongst the major contributors to folate intake in the UK diet. *Br. J. Nutr.* **2002**, *88*, 681–688.
(20) Oey, I.; Verlinde, P.; Hendrickx, M.; Van Loey, A. Temperature and pressure stability of L-ascorbic acid and/or [6S] 5-methyltetrahydrofolic acid: a kinetic study. *Eur. Food Res. Technol.* **2006**, *223*, 71–77.
(21) Le Noble, W. Kinetics of reactions in solutions under pressure. *Prog. Phys. Org. Chem.* **1967**, *5*, 207–329.
(22) Konings, E. A validated liquid chromatographic method for determining folates in vegetables, milk powder, liver, and flour. *J. AOAC Int.* **1999**, *82*, 119–127.
(23) Hawley, S. A. Reversible pressure−temperature denaturation of chymotrypsinogen. *Biochemistry* **1971**, *10*, 2436–2442.
(24) van Boekel, M. A. J. S. *Kinetic Modeling of Reactions in Foods*; CRC Press Taylor & Francis Group: Boca Raton, FL, 2009.
(25) Sengers, J.; Kamgar-Parsi, B. Representative equations for the viscosity of water substance. *J. Phys. Chem. Ref. Data* **1984**, *13*, 185–205.
(26) Gapski, G.; Whiteley, J.; Huennekens, F. Hydroxylated derivatives of 5-methyl-5,6,7,8-tetrahydrofolate. *Biochemistry* **1971**, *10*, 2930–2934.
(27) Blair, J. A.; Pearson, A. J.; Robb, A. J. Autoxidation of 5-methyl-5,6,7,8-tetrahydrofolic acid. *J. Chem. Soc., Perkin Trans. 2* **1975**, *1*, 18−21
(28) Stewart, W.; Shon, Y.; Box, G. Discrimination and goodness of fit of multiresponse mechanistic models. *AIChE J.* **1998**, *44*, 1404–1412.
(29) Chen, T.; Cooper, R. Thermal destruction of folacin—effect of ascorbic-acid, oxygen and temperature. *J. Food Sci.* **1979**, *44*, 713–716.
(30) Paine-Wilson, B.; Chen, T. Thermal destruction of folacin - Effect of pH and buffer ions. *J. Food Sci.* **1979**, *44*, 717–722.
(31) Stokes, P.; Webb, K. Analysis of some folate monoglutamates by high-performance liquid chromatography-mass spectrometry. I. *J. Chromatogr., A* **1999**, *864*, 59–67.
(32) Nelson, B.; Dalluge, J.; Margolis, S. Preliminary application of liquid chromatography−electrospray−ionization mass spectrometry to the detection of 5-methyltetrahydrofolic acid monoglutamate in human plasma. *J. Chromatogr., B* **2001**, *765*, 141–150.
(33) Pawlosky, R.; Flanagan, V.; Pfeiffer, C. Determination of 5-methyltetrahydrofolic acid in human serum by stable-isotope dilution high-performance liquid chromatography−mass spectrometry. *Anal. Biochem.* **2001**, *298*, 299–305.
(34) Whiteley, J. M.; Russell, A. Structural reassignment of the peroxide oxidation product of 5-methyl-5,6,7,8-tetrahydrofolate. *Biochem. Biophys. Res. Commun.* **1981**, *101*, 1259–1265.
(35) Poe, M.; Hensens, O. D.; Hoogsteen, K. 5-Methyl-5,6,7,8-tetrahydrofolic acid. Conformation of the tetrahydropyrazine ring. *J. Biol. Chem.* **1979**, *254*, 10881–10884.
(36) Patro, B. S.; Adhikari, S.; Mukherjee, T.; Chattopadhyay, S. Possible role of hydroxyl radicals in the oxidative degradation of folic acid. *Bioorg. Med. Chem. Lett.* **2005**, *15*, 67–71.
(37) Ehrenberg, A.; Hemmerich, P.; Muller, F.; Pfleiderer, W. Electron spin resonance of pteridine radicals and the structure of hydropteridines. *Eur. J. Biochem.* **1970**, *16*, 584–591.
(38) Kirsch, M.; Korth, H.-G.; Stenert, V.; Sustmann, R.; de Groot, H. The autoxidation of tetrahydrobiopterin revisited. Proof of superoxide formation from reaction of tetrahydrobiopterin with molecular oxygen. *J. Biol. Chem.* **2003**, *278*, 24481–24490.
(39) Marshall, W. L.; Franck, E. U. Ion product of water substance, 0−1000 °C, 1−10000 bar. New international formulation and its background. *J. Phys. Chem. Ref. Data* **1981**, *10*, 295–304.

Received March 11, 2009. Revised manuscript received May 19, 2009. Accepted May 23, 2009. This work is supported by the Institute for the Promotion of Innovation through Science and Technology in Flanders (doctoral grant P.V., IWT—Vlaanderen) and the Research Foundation-Flanders (postdoctoral grant I.O., FWO—Vlaanderen).